

Effects of preparation temperature on electrochemical performance of nitrogen-enriched carbons

Chun WU, Xian-you WANG, Qing-lan ZHAO, Jiao GAO, Yan-song BAI, Hong-bo SHU

Key Laboratory of Environmentally Friendly Chemistry and Applications of Minister of Education,
School of Chemistry, Xiangtan University, Xiangtan 411105, China

Received 14 January 2014; accepted 27 February 2014

Abstract: The activated nitrogen-enriched novel carbons (NENCs) were prepared by direct carbonization using polyaniline coating activated mesocarbon microbead composites as the precursor. Herein the influences of the carbonization temperature on the structure and morphology of the NENCs samples were investigated by scanning electron microscopy (SEM), transmission electron microscopy (TEM), Fourier transform infrared spectroscopy (FTIR), X-ray diffraction (XRD), X-ray photoelectron spectroscopy (XPS) and N_2 adsorption/desorption isotherm at 77 K. The electrochemical properties of the supercapacitors were characterized by cyclic voltammetry, galvanostatic charge/discharge, electrochemical impedance spectroscopy (EIS), cycle life, leakage current and self-discharge measurements in 6 mol/L KOH solution. The results demonstrate that the NENC samples carbonized at 600 °C show the highest specific capacitance of 385 F/g at the current density of 1 A/g and the lowest ESR value (only 0.93 Ω). Furthermore, the capacity retention ratio of the NENCs-600 supercapacitor is 92.8 % over 2500 cycles.

Key words: carbonization temperatures; nitrogen-enriched novel carbon material; electrode active materials; supercapacitor

1 Introduction

As a new type of charge storage devices, supercapacitors possess many remarkable characteristics, such as low equivalent series resistance (ESR), long charge/discharge life and high power density [1,2], which have attracted more and more attentions owing to their wide range of potential applications, such as hybrid power sources for electric vehicles, digital telecommunication systems and pulse laser technique [3]. Various carbon materials including activated carbon [4,5], carbon aerogels [6] and mesoporous carbon [7] are the most frequently used electrode materials for supercapacitors because of their high surface area, good electronic conductivity and excellent stability [8,9]. The large specific surface area and the porosity of the activated carbon are the basic requirements to achieve the quick formation of a double-layer which results in high power density and long durability of these supercapacitors, also termed electric double-layer capacitors (EDLC) [10]. Besides, it is found that nitrogen-

enriched carbon materials can also be used as electrode materials for supercapacitors due to the inducing electron-donor properties of nitrogen functionalities [11,12]. The introduction of nitrogen could produce a pseudo capacitance besides the electric double-layer capacitance, enhance the wettability in electrode-electrolyte interface, and then improve the capacitance of electrode [13]. The carbonization of conducting polymers, such as polyaniline (PANI), is one of the methods to prepare nitrogen-enriched carbon materials. LI et al [14] prepared nitrogen-enriched mesoporous carbon spheres with a specific capacitance of 211 F/g at a discharge current density of 1 A/g. ROZLÍVKOVÁ et al [15] prepared the nitrogen-enriched carbon via carbonizing the PANI base in an inert atmosphere at temperatures up to 800 °C. Carbonization at 650 °C for 1 h has been suggested for the optimum conversion condition of PANI to carbon. MENTUS et al [16] revealed that the nitrogen-enriched carbon can be prepared through PANI in nitrogen atmosphere at a heating rate of 10 °C/min up to a maximum temperature of 800 °C. And the carbonized materials display the very high conductivity.

Foundation item: Projects (51072173, 51272221) supported by the National Natural Science Foundation of China; Project (20094301110005) supported by Specialized Research Fund for the Doctoral Program of Higher Education, China; Project (2013FJ4062) supported by Science and Technology Plan Foundation of Hunan Province, China

Corresponding author: Xian-you WANG; Tel: +86-731-58292060; E-mail: wxianyou@yahoo.com

DOI: 10.1016/S1003-6326(14)63499-3

In our previous work, the activated nitrogen-enriched novel carbons (NENCs) were successfully prepared by direct carbonization method using polyaniline/activated mesocarbon microbeads (PANI/ACMB) composites as the precursor [17]. In addition, the effects of activated treatment on the electrochemical performances of NENCs electrode materials and the electrochemical capacitive behaviors of the activated NENCs supercapacitors in various aqueous electrolytes were studied [18,19]. It has been well known that the carbonization temperatures for the activated NENCs will apparently affect their physical and electrochemical performances. To the best of our knowledge, the effects of carbonization temperatures on the microstructure and electrochemical performance of such a carbon material from the carbon-conducting polymer composites for supercapacitors have been rarely reported. Therefore, the effects of carbonization temperatures on physical and electrochemical properties of NENCs were further investigated in detail.

2 Experimental

2.1 Preparations of PANI/ACMB composites and NENCs

The PANI/ACMB composites were prepared using sodium dodecyl sulfate (SDBS) as the surfactant by chemical oxidation polymerization [20,21]. The experimental setup used for synthesis of PANI/ACMB composites have been reported in our previous work [17].

The as-prepared PANI/ACMB composites were carbonized at a heating rate of 5 °C/min under pure Ar, they were heated to the ultimate temperatures of 500, 600 and 700 °C, respectively, and maintained at the desired temperature for 2 h to form nitrogen-enriched carbon materials. Finally, the resultant carbon materials were activated in 16 mol/L HNO₃ at 70 °C for 24 h. The activated NENCs could be acquired after being washed to be neutral and dried in oven at 100 °C. The heated samples were named as NENCs-500, NENCs-600 and NENCs-700, respectively.

2.2 Preparation of carbon sample electrodes

The electrodes materials, as usually in such devices, consisted of 80% carbon sample (mass fraction), 10% acetylene black and 10% polyvinylidene fluoride (PVDF). After being well mixed, the mixtures were blended to obtain slurries. Then the slurries were coated on nickel foams that were used as current collectors and dried in vacuum overnight at 120 °C. Finally, the nickel foams were pressed under a pressure of 1.6×10^7 Pa. The geometric surface area of the electrodes was kept to be 1.0 cm².

2.3 Characterization of materials

The surface morphologies and microstructures of the NENCs samples can be examined using the scanning electron microscopy (SEM, JSE-6360LV) and transmission electron microscopy (TEM, JEM-2100F, JEOL).

The sample was characterized via the Fourier transform infrared (FTIR) spectrometer (Perkin-Elmer spectrum one).

X-ray diffraction (XRD) analysis was done using a diffractometer (D/MAX-3C, Rigaku, Japan) with Cu K_α radiation ($\lambda=1.5406$ Å) and a graphite monochromator at 40 kV, 300 mA. The scanning rate is 8 (°)/min and the scanning range of diffraction angle (2θ) is $10^\circ \leq 2\theta \leq 80^\circ$.

The surface characteristics of the nanocomposites were finished by X-ray photoelectron spectroscopy (XPS) (K-Alpha 1063, Thermo. Fisher Scientific, Britain).

The NENCs were examined by adsorption experiments of nitrogen, and the adsorption/desorption isotherms of nitrogen were measured at 77 K on a Quantachrome autosorb automated gas sorption system.

2.4 Electrochemical measurements

The electrochemical behaviors of the as-prepared sample electrodes, which were impregnated in 6 mol/L KOH electrolyte, were investigated by cyclic voltammetry, galvanostatic charge/discharge test and electrochemical impedance spectroscopy (EIS) conducted on a CHI660 electrochemical workstation (CH Instruments, USA). The measurements were carried out in a standard three-electrode cell system, in which nickel and the Hg/HgO electrodes (SCE) were used as counter and reference electrodes via a luggin capillary with a salt bridge, respectively. The voltage range for CV test varied from -1 to 0 V. While the voltage range for the galvanostatic measurement varied from 0 to 1 V at the current density from 1 to 5 A/g. The electrochemical impedance spectroscopy (EIS) in the frequency ranges from 10⁵ Hz to 10⁻² Hz with amplitude of 5 mV. Moreover, the cycle life, leakage current and self-discharging measurements were carried out by potentiostat/galvanostat (BTS 6.0, Neware, Guangdong, China) on button supercapacitor. The symmetrical button supercapacitors were assembled according to the order of electrode–separator–electrode.

3 Results and discussion

3.1 Structure analysis

The morphologies of PANI/ACMB composites and NENCs samples are shown in Figs. 1(a)–(d). It can be seen that the as-synthesized PANI/ACMB composites possess the leech-like morphology with coarse external surface (Fig. 1(a)). Meanwhile, it is not difficult to find

that the whisker-like morphology appears on the coarse external surface of NENCs samples after being carbonized. With the increase of carbonization temperature, the whisker-like morphology becomes more and more evident. The reasons may be the breakage of some chemical bonds and partial oxidation of carbon surface. However, when the temperature increases from 600 °C to 700 °C, the microspheres aggregate severely (Fig. 1(d)). It demonstrates that the structure and morphology of the NENCs samples can be greatly affected by the carbonization temperatures.

The TEM images of PANI/ACMB composites and NENCs-600 are shown in Figs. 2(a) and (b), in which the morphology of the NENCs-600 is similar to that of PANI/ACMB composites, but there is a slight decrease of covering thickness on the external surface of the ACMB for the NENCs-600. This is caused by the shrinkage of PANI due to the release of non-carbon

elements such as N and O during the carbonization process. The external surfaces keep coarse with the change of the carbonization temperatures, thus significantly offering the chance contacting between electrode materials and electrolyte, and inducing better electrochemical performance.

Figure 3 shows the FTIR spectra of the PANI/ACMB composites and NENCs samples. The key characteristic peaks of PANI/ACMB composites corresponding to the quinoid ring and the benzene ring are observed at 1574.6 and 1492 cm^{-1} , respectively. The other peaks at 1281.1 and 1121.7 cm^{-1} can be assigned to the C—N stretching of the secondary aromatic amine and aromatic C—H in-plane bending, respectively [22]. The 1248 cm^{-1} band could be thought to be a C—N—C stretching vibration in the polaron structure. The N=Q=N stretching band at 1115.6 cm^{-1} is ascribed to the characteristic band of polyaniline base [23]. While

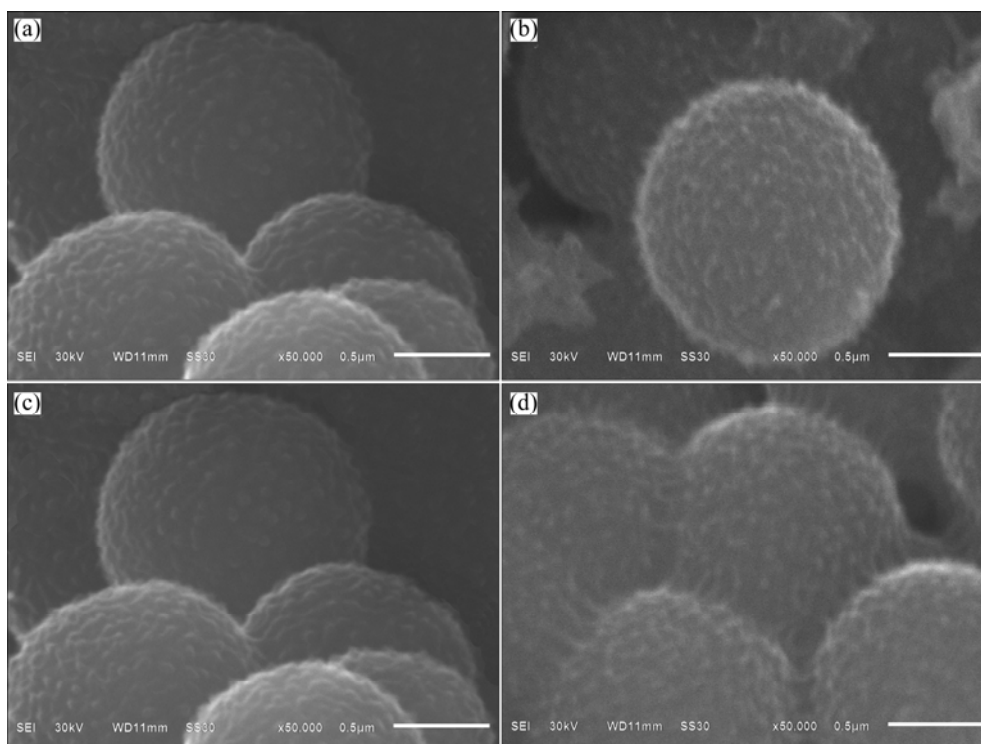


Fig. 1 SEM images of PANI/ACMB composites (a), NENCs-500 (b), NENCs-600 (c) and NENCs-700 (d)

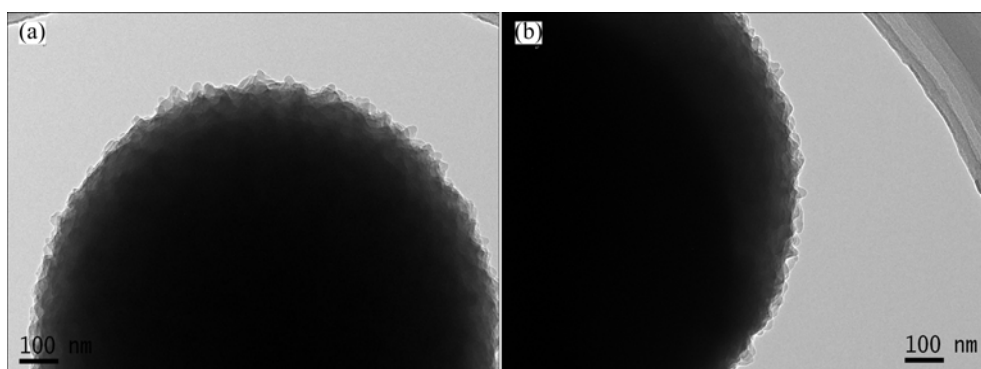


Fig. 2 TEM images of PANI/ACMB composites (a) and NENCs-600 (b)

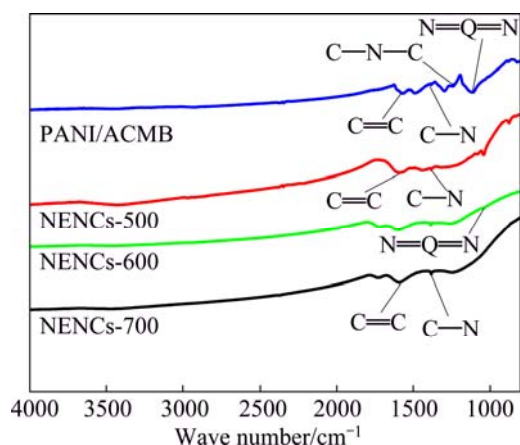


Fig. 3 FTIR spectra of PANI/ACMB composites and NENCs samples

for the spectra of different NENCs samples, the spectra of NENCs-500 and NENCs-600 similarly display with that of PANI/ACMB, the 1593.6 cm^{-1} band is assigned to the C=C stretching vibration and the N=Q=N stretching band at 1046.7 cm^{-1} is ascribed to the characteristic band of polyaniline base, respectively. With the increase of carbonization temperature, nitrogen as a heteroatom is volatilized. The N=Q=N stretching band of NENCs-700 disappears. Meanwhile, the C—N stretching peaks at 1389 cm^{-1} of NENCs-700 gradually becomes weaker. These results will be confirmed by XRD and XPS analyses.

The XRD patterns of PANI/ACMB composites and NENCs samples are shown in Fig. 4. Two broad peaks at 2θ of 20° and 25° can be ascribed to the periodicity parallel and perpendicular to the polymer chains of PANI in PANI/ACMB composites [24]. After being carbonized at different temperatures, the XRD patterns of different NENCs samples exhibit two broad diffraction peaks around 24° and 43° , which correspond to the (002) and (100) diffraction peaks of graphite, respectively [25]. At

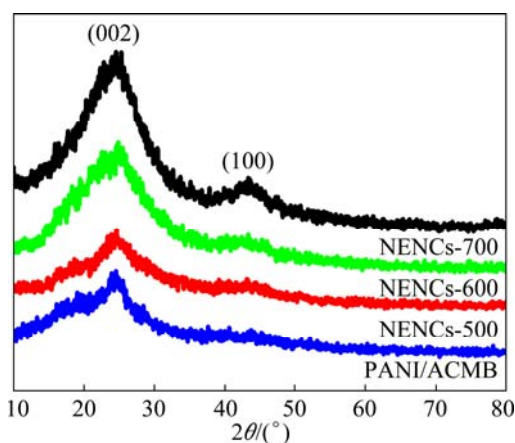


Fig. 4 XRD patterns of PANI/ACMB composites and different NENCs samples

the same time, when the carbonization temperature increases to $600\text{ }^\circ\text{C}$, the (002) and (100) peaks become somewhat narrow and shift to higher angles. Compared with NENCs-500, the intensity of the (100) peak for NENCs-600 is gradually enhanced, revealing the improvement of the graphitization degree, while the heteroatom of nitrogen is volatilized with the increase of temperature.

XPS is also performed to characterize the elemental composition of the electrode materials. In order to further analyze the contents of oxygen and nitrogen in NENCs samples prepared at different carbonization temperatures, the typical XPS spectra of N1s and O1s are shown in Fig. 5, and the contents of carbon, oxygen and nitrogen for samples are listed in Table 1. From Fig. 5, the O1s spectra of the samples reveal the presence of three peaks [26,27] corresponding to carbonyl type groups and/or quinone (O-I) (peak 1, BE=531.0–531.1 eV), C—OH (O-II) and/or C—O—C groups (O-III) (peaks 2 and 3, BE=532 and 532.4–533.1 eV), respectively. The chemical state of nitrogen atoms in carbonized samples could be assigned to four types according to previous reports [28]. These four types are indexed as following binding energies: pyridinic nitrogen (N-6) or graphene nitrogen (peak 1, BE=398.7±0.3 eV), pyrrolic nitrogen and pyridinic nitrogen in association with oxygen functionality or conjugated nitrogen (N-5) (peak 2, BE=400.3±0.3 eV), quaternary nitrogen, nitrogen substituted with carbons in the aromatic grapheme structure (N-Q) (peak 3, BE=401.4±0.5 eV), chemisorbed nitrogen oxides—N—Ox (N-X) (peak 4, BE=405.8 eV) [29]. The reversibility of the material mainly results from the graphene nitrogen, and the higher the content of nitrogen is, the higher the capacity is [29]. As listed in Table 1, the oxygen and nitrogen contents in the NENCs samples decrease with the increase of carbonization temperature, which is in agreement with FTIR and XRD analysis.

In addition, the relative surface concentrations of different O1s and N1s are listed in Table 1. The comparisons of O1s and N1s for the different NENCs samples have shown that although all the samples have the same contributions, the types and contribution of particular oxygen and nitrogen species differ significantly at the different carbonization temperatures. According to the previous study [30], O-I and nitrogen located at the edges of graphene layers, that is, N-6 and N-5, are considered to lead to the pseudocapacitance effect. The percentages of O-I and N-5 in NENCs-600 are higher than those of the other two samples. Therefore, it can be expected that the NENCs-600 will possess more excellent electrochemical performance.

Figure 6 shows the N_2 adsorption/desorption isotherms of different NENCs samples. The isotherms

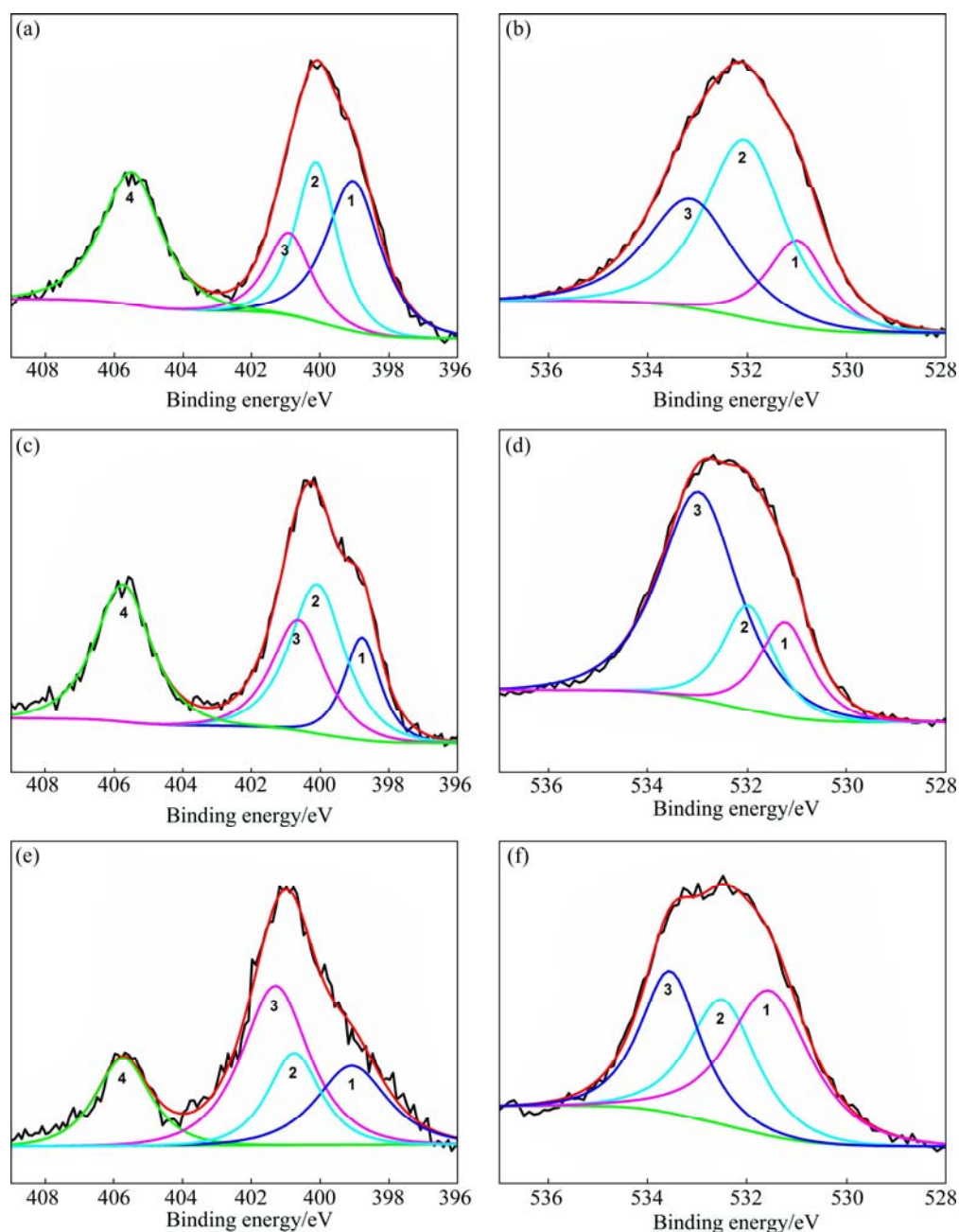


Fig. 5 Fitted high-resolution XPS spectra of different NENCs samples: (a) NENCs-500, N1s spectrum; (b) NENCs-500, O1s spectrum; (c) NENCs-600, N1s spectrum; (d) NENCs-600, O1s spectrum; (e) NENCs-700, N1s spectrum; (f) NENCs-700, O1s spectrum

Table 1 Contents of carbon, oxygen and nitrogen of different NENCs samples (mass fraction, %)

Sample	C	O	N	Nitrogen content				Oxygen content		
				N-X	N-Q	N-5	N-6	O-I	O-II	O-III
NENCs-500	69.9	20.9	9.2	2.7	1.3	2.3	2.9	3.8	10.2	6.9
NENCs-600	72.6	19.2	8.2	2.5	1.9	2.6	1.2	11.7	4.0	3.5
NENCs-700	85.5	12.1	2.4	0.5	0.5	1.0	0.4	3.5	5.0	3.6

for different NENCs samples are typical type I according to IUPAC classification, indicating that all the NENCs samples are microporous structure. The micropores participate in charge storage process of supercapacitors

by providing abundant adsorbing sites for the ions [31]. Meanwhile, the NENCs-600 shows much higher specific surface area of 420.0 m²/g compared with the NENCs-500 (265.2 m²/g). In general, a large surface area

is necessary for charge accumulation for a high energy density EDLC electrode material. In the case of NENCs-700, high temperature will increase the degree of graphitization and cut down porosity, therefore NENCs-700 displays lower specific surface area of 403.9 m^2/g .

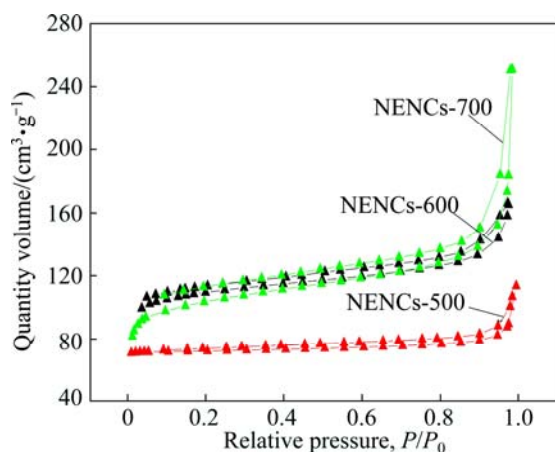


Fig. 6 Nitrogen adsorption/desorption isotherms of different NENCs samples

3.2 Measurements of electrochemical performance

Figure 7(a) shows the CV curves of different NENCs samples at a scan rate of 2 mV/s . All the voltammetric curves are close to rectangular shape, which indicates that the activated NENCs acting as EDLCs electrodes have excellent reversibility in aqueous electrolyte [32]. However, small humps during the sweep between -0.4 and -0.8 V are clearly observed, which is usually attributed to Faradic reactions involving the quinone functional groups [33]. The nitrogen-enriched functional groups, especially the pyrrolic and pyridinic nitrogen have been reported to be electrochemically active in the Faradaic reactions [27]. Nitrogen-enriched functionalities have generally basic characterization, inducing electron-donor properties. These electrochemically active centers could contribute to the pseudocapacitance, which generally originates from the Faradaic interactions between the potassium cations in the KOH solution and the nitrogen atoms of carbon materials [34]. Moreover, the curve area of NENCs-600 is larger than that of the others, suggesting that the specific capacitance of the former is higher than that of the latter.

Figure 7(b) further shows the comparisons of the specific capacitance values depending on the scan rates (1–10 mV/s) and temperatures (500–700 $^{\circ}\text{C}$) for all the electrodes. It can be noted that the specific capacitances firstly increase and then decrease with the increase of the temperatures at the same scan rate. The excellent performance of NENCs-600 corresponds to the higher specific surface area and appropriate oxygen and

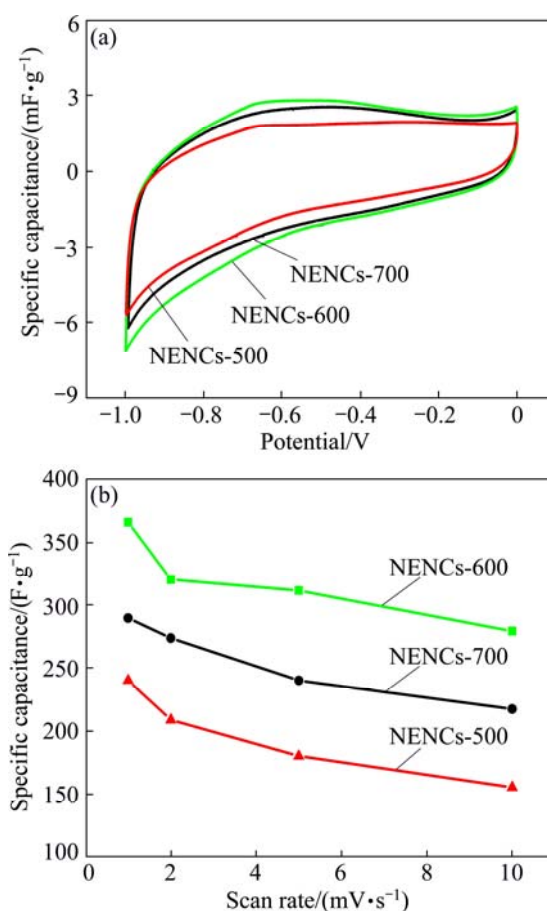


Fig. 7 CV curves of different NENC electrodes at scan rate of 2 mV/s (a) and specific capacitance of different NENC electrodes at different scan rates (b)

nitrogen content. The higher specific surface area can significantly provide the chance contacting between electrode materials and electrolyte, resulting in the increase of double-layer capacitance. While, the appropriate oxygen and nitrogen content in NENCs-600 contributes to the pseudocapacitance. Although the oxygen and nitrogen contents of NENCs-500 are the highest, the specific capacitance is lower than that of NENCs-700. This is ascribed to its lower surface area and graphitization degree, which supplies lower electric double-layer capacitance. On the other hand, with the increase of the scan rate, the capacitances of the same NENCs electrodes are slowly degraded. However, for the NENCs-600 electrode, even at the high scan rate of 10 mV/s the capacitance is still about 279.3 F/g , which is much higher than that of the other two samples. Therefore, the NENCs-600 sample possesses the best rate capability among the NENCs samples. The capacitance values can be determined by the equation as follows [35]:

$$C_{s,t} = \frac{I_a + |I_c|}{2m(dV/dt)} \quad (1)$$

where $C_{s,t}$ is the specific capacitance (F/g); I_a and I_c are the current (A) of anodic and cathodic voltammetric curves on positive and negative sweeps, respectively; m is the mass of the material (g) (only including the mass of the NENCs samples, the same below); dV/dt is the sweep rate (mV/s).

Figure 8 shows the galvanostatic charge/discharge curves of different NENC electrodes measured at the current densities of 1 A/g in 6 mol/L KOH between 0 and 1 V. The variations of the curves are not linear relationship with the charge/discharge time and give rise to an inflexion, and this inflexion further verifies that the oxygen and nitrogen atoms of carbon materials can offer a pseudocapacitance effect. Furthermore, the curve of the NENCs-600 shows longer discharge time than the others, which means higher specific capacitance in 6 mol/L KOH at current density of 1 A/g. Meanwhile, the specific capacitances of the NENCs-500, NENCs-600 and NENCs-700 samples are 248.6, 385 and 301.1 F/g, respectively, indicating that the pseudocapacitance of oxygen and nitrogen makes a significant contribution. The values can be evaluated from the slope of the charge/discharge curves, according to the equation as follows [23]:

$$C_m = \frac{i \cdot t_d}{m \Delta V} \quad (2)$$

where C_m is the specific capacitance (F/g); i is the charge/discharge current (A); ΔV is the potential range of the charge/discharge (V); t_d is the discharge time (s); m is the mass of active material (g) within the electrode.

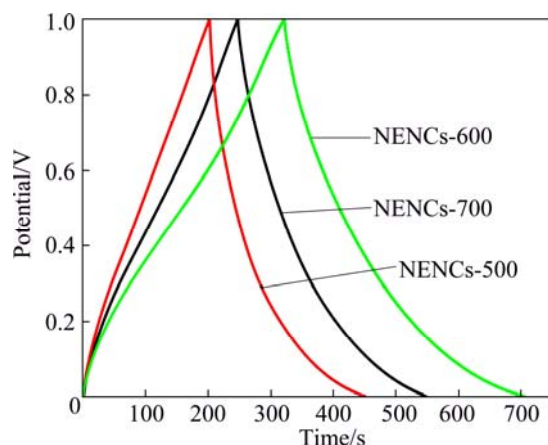


Fig. 8 Galvanostatic charge/discharge curves of different NENC electrodes at current density of 1 A/g

The electrochemical impedance spectroscopy (EIS) was used to further analyze the electrochemical properties about characteristic frequency responses. Figure 9 shows the AC impedance spectra (Nyquist plots) responding to frequency for different NENC electrodes. It can be found that there is a straight line in the

low-frequency region (lower than 100 Hz) because of Warburg impedance, which is a result of the frequency dependence of ion diffusion in the electrolyte to the electrode interface [36,37]. Obviously, the NENCs-600 electrode with an almost vertical line is rather different from those of NENCs-500 and NENCs-700 electrodes with a nearly 45° line, which is owing to the electrolyte easily to penetrate into the pores of the NENCs-600 [38]. In addition, the Warburg curve of NENCs-600 is shorter than other reported supercapacitor electrodes [2], which indicates that the NENCs-600 has a fast ion transport rate. This shall facilitate the efficient access of electrolyte ions to the inner of activated material [39]. Furthermore, the impedance in high frequency (the inset of Fig. 9) has an inconspicuous arc-shaped curve due to the ESR, namely the equivalent series resistance consisting of electronic contributions and ionic contributions. The ESR value of NENCs-600 is estimated to be around 0.93 Ω from the crossover point of the highest frequency with the real part of the impedance, which is lower than that of the other two samples (1.22 Ω for NENCs-500 and 1.12 Ω for NENCs-700, respectively). The results demonstrate that the NENCs-600 possesses excellent capacitive performance, which is in agreement with the above tests.

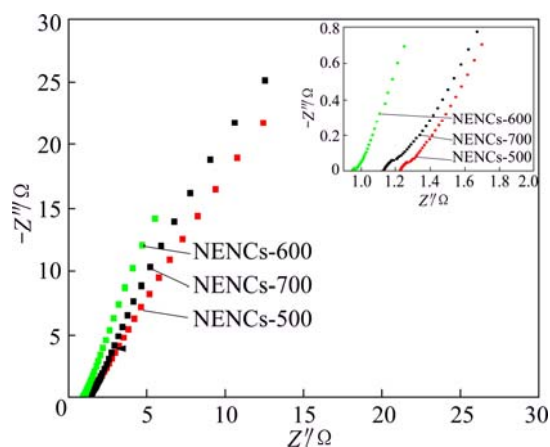


Fig. 9 Nyquist plot based on different NENC electrodes in frequency range of 10^5 to 10^{-2} Hz (the inset shows expanded high-frequency region)

Long cycle life of the supercapacitor is paramount evaluation for practical applications. Figure 10 shows the change of specific capacitance versus cycle number for different NENCs samples at the constant charge/discharge density of 500 mA/g. Apparently, the specific capacitances of the NENCs supercapacitors increase gradually at the beginning of cycles due to an initial activation process for Faradaic pseudocapacitance of the materials. During the middle cycle process, the values of the specific capacitance fluctuate a little, which is attributed to the instability of the oxygen and nitrogen functional groups. As for the NENCs-600, the maximum

specific capacitance reaches 89.5 F/g. After 2500 consecutive cycles, the specific capacitance keeps still at 57.8, 83.1 and 65.6 F/g for the NENCs-500, NENCs-600 and NENCs-700, respectively. The capacity retention ratio of the NENCs-600 is as high as 92.8%. These data illustrate that the supercapacitors using different NENCs as electrode active materials all present good cycling stability in the repetitive charge/discharge cycling. Particularly, supercapacitor using the NENCs-600 as electrode active material exhibits excellent cyclic stability.

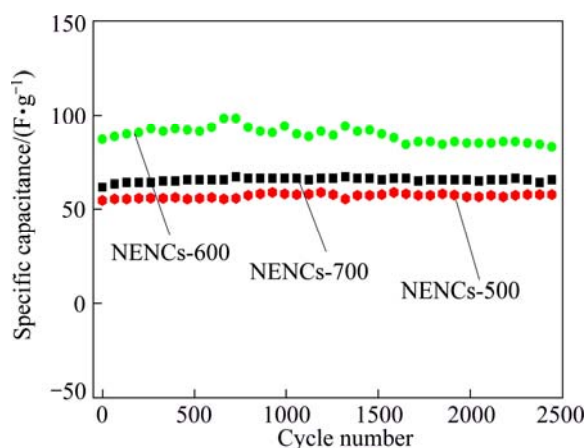


Fig. 10 Charge/discharge cycle performance of different NENC supercapacitors at a current density of 500 mA/g

As it is well-known, the leakage current and self-discharge of supercapacitor are also vital parameters for the application of supercapacitor. Figure 11 shows the leakage current and self-discharge curves of the NENCs-500, NENCs-600 and NENCs-700 supercapacitors. It can be noted from Fig. 11(a) that the leakage current drops rapidly before 15 min and stays at 0.040, 0.034 and 0.037 mA for the NENCs-500, NENCs-600 and NENCs-700 supercapacitors, respectively. As a result of the leakage current, the open circuit voltage of supercapacitor reduces gradually with the extending of time, and it decreases quickly before 4 h and becomes gentle subsequently. Obviously, the NENCs-600 supercapacitor exhibits the lowest self-discharge rate with the potential of 0.67 V after 720 min. The phenomenon can be explained that the biggish leakage currents and self-discharge are caused when the diffusion layer ions regress to bulk solution at the beginning and the compact layer ions move to diffusion layer because of vibration and concentration difference. As the moving velocity is slow, the leakage current and self-discharge keep relatively jarless and become small after some time [2]. These results demonstrate that the NENCs-600 supercapacitor possesses the best electrochemical performances.

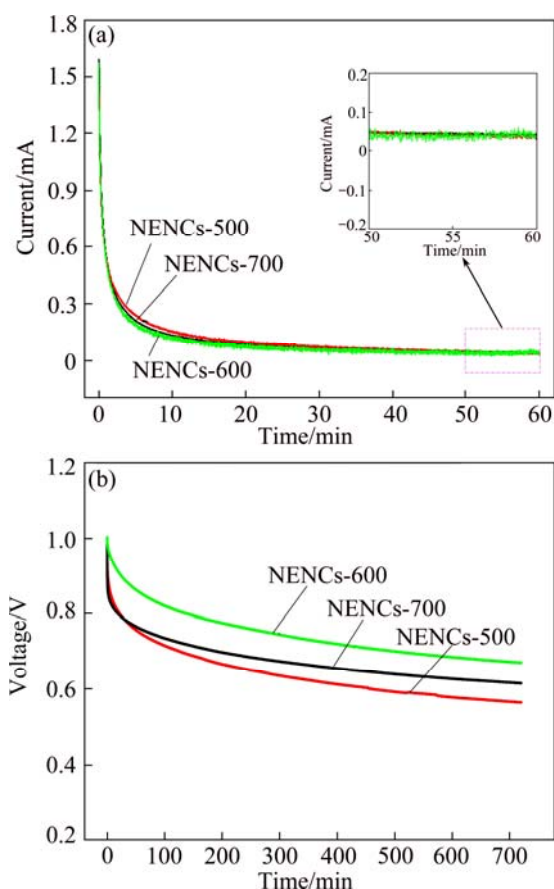


Fig. 11 Leakage current (a) and self-discharge (b) of different NENC supercapacitors for different time

4 Conclusions

1) The carbonization temperatures have marked effects on both the structure and the electrochemical performances of the NENC samples. All of the NENCs present remarkable supercapacitive behaviors, small ohmic resistance and long cycle life.

2) The NENC sample carbonized at 600 °C shows the highest specific capacitance of 385 F/g at the current density of 1 A/g. Furthermore, the specific capacitance of the button supercapacitor using the NENCs-600 electrode is as high as 89.5 F/g at the charge/discharge current density of 500 mA/g and exhibits the lowest self-discharge rate.

3) The good electrochemical performance can be ascribed to the higher specific surface area and the presence of oxygen and nitrogen functional groups. Therefore, the NENCs-600 will be a kind of potential electrode active materials for the application of high performance supercapacitors.

References

- [1] BURKE A. Ultracapacitors: Why, how, and where is the technology [J]. *Journal of Power Sources*, 2000, 91(1): 37–50.

- [2] ZHOU S Y, LI X H, WANG Z X, GUO H J, PENG W J. Effect of activated carbon and electrolyte on properties of supercapacitor [J]. Transactions of Nonferrous Metals Society of China, 2007, 17(6): 1328–1333.
- [3] FRACKOWIAK E, BÉGUIN F. Carbon materials for the electrochemical storage of energy in capacitors [J]. Carbon, 2001, 39(6): 937–950.
- [4] LOZANO-CASTEOL D, CAZORLA-AMOROS D, LINARES-SOLANO A, SHIRAIISHI S, KURIHARA H, OYA A. Influence of pore structure and surface chemistry on electric double layer capacitance in non-aqueous electrolyte [J]. Carbon, 2003, 41(9): 1765–1775.
- [5] WANG X F, RUAN D B, YOU Z. Applications of spherical Ni(OH)₂/CNTs composite electrode in asymmetric supercapacitor [J]. Transactions of Nonferrous Metals Society of China, 2006, 16(5): 1129–1134.
- [6] LI W, REICHENAUER G, FRICHE J. Carbon aerogels derived from cresol-resorcinol-formaldehyde for supercapacitors [J]. Carbon, 2002, 40(15): 2955–2959.
- [7] YAN X, SONG H H, CHEN X H. Synthesis of spherical ordered mesoporous carbons from direct carbonization of silica/triblock-copolymer composites [J]. Journal of Materials Chemistry, 2009, 19(26): 4491–4494.
- [8] ZHANG L L, ZHAO X S. Carbon-based materials as supercapacitor electrodes [J]. Chemical Society Reviews, 2009, 38(9): 2520–2531.
- [9] FRACKOWIAK E. Carbon materials for supercapacitor application [J]. Physical Chemistry Chemical Physics, 2007, 9(15): 1774–1785.
- [10] PANDOLFO A G, HOLLENKAMP A F. Carbon properties and their role in supercapacitors [J]. Journal of Power Sources, 2006, 157(1): 11–27.
- [11] QIN C L, LU X, YIN G P, BAI X D, JIN Z. Activated nitrogen-enriched carbon/carbon aerogel nanocomposites for supercapacitor applications [J]. Transactions of Nonferrous Metals Society of China, 2009, 19(S3): s738–s742.
- [12] WANG F X, XIAO S Y, HOU Y Y, HU C L, LIU L L, WU Y P. Electrode materials for aqueous asymmetric supercapacitors [J]. RSC Advances, 2013, 3(32): 13059–13084.
- [13] KAWAGUCHI M, ITOH A, YAGI S, ODA H. Preparation and characterization of carbonaceous materials containing nitrogen as electrochemical capacitor [J]. Journal of Power Sources, 2007, 172(1): 481–486.
- [14] LI W R, CHEN D H, LI Z, SHI Y F, WAN Y, HUANG J J, YANG J J, ZHAO D Y, JIANG Z Y. Nitrogen enriched mesoporous carbon spheres obtained by a facile method and its application for electrochemical capacitor [J]. Electrochemistry Communications, 2007, 9(4): 569–573.
- [15] ROZLÍVKOVÁ Z, TRCHOVÁ M, EXNEROVÁ M, STEJSKAL J. The carbonization of granular polyaniline to produce nitrogen-containing carbon [J]. Synthetic Metals, 2011, 161(11): 1122–1129.
- [16] MENTUS S, ČIRIĆ-MARJANOVIĆ G, TRCHOVÁ M, STEJSKAL J. Conducting carbonized polyaniline nanotubes [J]. Nanotechnology, 2009, 20(24): 245601–245611.
- [17] WU C, WANG X Y, JU B W, ZHANG X Y, JIANG L L, WU H. Supercapacitive behaviors of activated mesocarbon microbeads coated with polyaniline [J]. International Journal of Hydrogen Energy, 2012, 37(19): 14365–14372.
- [18] WU C, WANG X Y, JU B W, JIANG L L, WU H, ZHAO Q L, YI L H. Supercapacitive performance of nitrogen-enriched carbons from carbonization of polyaniline/activated mesocarbon microbeads [J]. Journal of Power Sources, 2012, 227: 1–7.
- [19] WU C, WANG X Y, JU B W, BAI Y S, JIANG L L, WANG H, ZHAO Q L, GAO J, WANG X Y, YI L H. Supercapacitive behaviors of the nitrogen-enriched activated mesocarbon microbead in aqueous electrolytes [J]. Journal of Solid State Electrochemistry, 2013, 17(6): 1693–1700.
- [20] KIM J H, LEE Y S, SHARMA A K, LIU C G. Polypyrrole/carbon composite electrode for high-power electrochemical capacitors [J]. Electrochimica Acta, 2006, 52(4): 1727–1732.
- [21] LU X F, MAO H, ZHANG W J. Fabrication of core-shell Fe₃O₄/polypyrrole and hollow polypyrrole microspheres [J]. Polymer Composites, 2009, 30(6): 847–854.
- [22] LI L X, SONG H H, ZHANG Q C, YAO J Y, CHEN X H. Effect of compounding process on the structure and electrochemical properties of ordered mesoporous carbon/polyaniline composites as electrodes for supercapacitors [J]. Journal of Power Sources, 2009, 187(1): 268–274.
- [23] WANG Y G, LI H Q, XIA Y Y. Ordered whiskerlike polyaniline grown on the surface of mesoporous carbon and its electrochemical capacitance performance [J]. Advanced Materials, 2006, 18(19): 2619–2623.
- [24] ZHANG Z M, WEI Z X, WAN M X. Nanostructures of polyaniline doped with inorganic acids [J]. Macromolecules, 2002, 35(15): 5937–5942.
- [25] PRESSER V, HEON M, GOGOTSI Y. Carbide-derived carbons-from porous networks to nanotubes and grapheme [J]. Advanced Functional Materials, 2011, 21(5): 810–833.
- [26] BINIAK S, SZYMANSKI G, SIEDLEWSKI J, SWIATKOWSKI A. The characterization of activated carbons with oxygen and nitrogen surface groups [J]. Carbon, 1997, 35(12): 1799–1810.
- [27] RUFFORD T E, HULICOVA-JURCAKOVA D, ZHU Z H, LU G Q. Nanoporous carbon electrode from waste coffee beans for high performance supercapacitors [J]. Electrochemistry Communications, 2008, 10(10): 1594–1597.
- [28] BAGREEV A, MENENDEZ J A, DUKHNO I, TARASENKO Y, BANDOSZ T J. Bituminous coal-based activated carbons modified with nitrogen as adsorbents of hydrogen sulfide [J]. Carbon, 2004, 42(3): 469–476.
- [29] WU Y P, FANG S B, JIANG Y Y. Effects of nitrogen on the carbon anode of a lithium secondary battery [J]. Solid State Ionics, 1999, 120(1–4): 117–123.
- [30] HULICOVA-JURCAKOVA D, SEREDYCH M, LU G Q, TERESA J B. Combined effect of nitrogen- and oxygen-containing functional groups of microporous activated carbon on its electrochemical performance in supercapacitors [J]. Advanced Functional Materials, 2009, 19(3): 438–447.
- [31] XIA K S, GAO Q M, JIANG J H, HU J. Hierarchical porous carbons with controlled micropores and mesopores for supercapacitor electrode materials [J]. Carbon, 2008, 46(13): 1718–1726.
- [32] ZHANG X Y, WANG X Y, SU J C, WANG X Y, JIANG L L, WU H, WU C. The effects of surfactant template concentration on the supercapacitive behaviors of hierarchically porous carbons [J]. Journal of Power Sources, 2012, 199: 402–408.
- [33] XIANG X X, LIU E H, LI L M, YANG Y J, SHEN H J, HUANG Z Z, TIAN Y Y. Activated carbon prepared from polyaniline base by K₂CO₃ activation for application in supercapacitor electrodes [J]. Journal of Solid State Electrochemistry, 2011, 15(3): 579–585.
- [34] HULICOVA D, KODAMA M, HATORI H. Electrochemical performance of nitrogen-enriched carbons in aqueous and non-aqueous supercapacitors [J]. Chemistry of Materials, 2006, 18(9): 2318–2326.
- [35] HU C C, WANG C C. Improving the utilization of ruthenium oxide within thick carbon–ruthenium oxide composites by annealing and anodizing for electrochemical supercapacitors [J]. Electrochemistry Communications, 2002, 4(7): 554–559.
- [36] QU D Y. Studies of the activated carbons used in double-layer supercapacitors [J]. Journal of Power Sources, 2002, 109(2): 403–411.

- [37] NISHINO A. Capacitors: Operating principles, current market and technical trends [J]. Journal of Power Sources, 1996, 60(2): 137–147.
- [38] SONG H K, HWANG H Y, LEE K H, DAO L H. The effect of pore size distribution on the frequency dispersion of porous electrodes [J]. Electrochimica Acta, 2000, 45(14): 2241–2257.
- [39] WANG Y, SHI Z Q, HUANG Y, MA Y F, WANG C Y, CHEN M M, CHEN Y S. Supercapacitor devices based on graphene materials [J]. The Journal of Physical Chemistry C, 2009, 113(30): 13103–13107.

制备温度对含氮碳材料电化学性能的影响

吴 春, 王先友, 赵青蓝, 高 娇, 白艳松, 舒洪波

湘潭大学 化学学院 环境友好化学与应用教育部重点实验室, 湘潭 411105

摘 要: 以聚苯胺包覆活性炭微球复合电极材料作为前驱体并进行高温碳化得到新型含氮碳材料(NENCs)。通过扫描电镜、透射电镜、傅里叶变换红外光谱、X 射线衍射、X 射线光电子能谱以及 77 K 温度下氮气吸脱附测试, 研究碳化温度对 NENCs 形貌和结构的影响。将其组装成超级电容器在 6 mol/L KOH 电解液中进行了循环伏安、充放电、交流阻抗、循环寿命、漏电流以及自放电测试。结果表明: 高温碳化得到的 NENCs 材料都具有很好的超级电容性能, 尤其是碳化温度为 600 °C 时得到的材料, 当电流密度为 1 A/g 时的放电比电容高达 385 F/g 且显示最低的等效串联电阻值; 且 2500 次循环后容量保持率高达 92.8%。

关键词: 碳化温度; 含氮碳材料; 电极活性材料; 超级电容器

(Edited by Chao WANG)